Soft Matter

PAPER

View Article Online
View Journal | View Issue

Cite this: *Soft Matter*, 2019, 15, 8329

A first porphyrin liquid crystal with strong fluorescence in both solution and aggregated states based on the AIE-FRET effect†

Hongyu Guo,[a] Sining Zheng,[a] Shibin Chen,[a] Chenyang Han[ab] and Fafu Yang *[ac]

Received 11th June 2019,
Accepted 13th September 2019

DOI: 10.1039/c9sm01174a

rsc.li/soft-matter-journal

Porphyrins are good near-infrared fluorescent materials, but the strong self-assembly stacking resulted in the aggregation-caused quenching (ACQ) effect, limiting their emissive performance in aggregated states. In this work, a novel diphenylacrylonitrile–porphyrin derivative with multiple polyglycol chains on the periphery was designed and synthesized as an excellent near-infrared-emissive liquid crystalline material in both solution and aggregated states, which was first observed for porphyrin liquid crystals. It exhibited a high self-assembly ability with the ordered hexagonal columnar mesophase between 70 and 120 °C approximately. The strong AIE-FRET effect was produced based on the overlap of the emission wavelength of diphenylacrylonitrile and the absorption wavelength of the porphyrin, resulting in the excellent near-infrared emission in both solution and aggregated states. The pseudo Stokes shift was as large as 210 nm and the fluorescence quantum yield reached 0.12 in the solid state. Moreover, this porphyrin liquid crystal displayed low biotoxicity and excellent fluorescence bio-imaging ability in living cells, opening a new application prospect for porphyrin liquid crystalline materials.

1. Introduction

Discotic liquid crystals, as important soft matter materials with excellent supramolecular self-assembly abilities of liquid–crystalline columnar mesophases, have been paid considerable research attention based on their distinctive features such as self-organization into self-healing of organizational defects, one-dimensional charge migration, and potential applications in thin film transistors, organic light emitting diodes and photovoltaic devices.[1–8] Among all kinds of columnar liquid crystals, the ones with high fluorescence had attracted much attention due to the effective combination of intrinsic luminescence capability and supramolecular self-assembly characteristic within a mesophase.[9,10] Up to now, a series of columnar liquid crystals with excellent fluorescence had been prepared, such as Bodipy liquid crystals,[11–14] perylene liquid crystals,[15–24] tristriazolotriazine liquid crystals,[25,26] metallomesogens,[27,28] *etc.* Although these fluorescence liquid crystals had been developed successfully, however, a survey of the literature suggested two obvious shortcomings for these studies. One was the weak even no fluorescence in aggregated states for these fluorescent liquid crystals because of the strong ACQ effect in aggregated states. Another was that the near-infrared fluorescent liquid crystal was seldom reported, which deserved to be investigated because the near-infrared materials had the advantages of high tissue penetration, low cell damage and little self-fluorescence interference of biological tissues, exhibiting potential applications in many research fields, such as telecommunications, thermal imaging, biological imaging and so on.[29,30] Thus, the near-infrared fluorescent liquid crystal with high emission in both solution and aggregated states is still a research challenge in the field of discotic liquid crystals.

On the other hand, it was well known that porphyrins were excellent near-infrared-emissive fluorescent materials with broad application prospects.[31] Based on their planar conjugated aromatic structures, some porphyrin liquid crystals and liquid porphyrins were also reported by introducing long alkyl chains on the periphery of the porphyrin skeleton.[32–46] However, although these reported porphyrin liquid crystals exhibited good fluorescence in various organic solutions, they did not exhibit good fluorescence behaviour in aggregated states due to the strong ACQ effect, limiting seriously further applications such as solid emission and bio-imaging in aqueous solution. Lately, in order to obtain porphyrin derivatives with solid fluorescence, the AIE (aggregate-induced emission) phenomena, which were discovered and studied extensively by Tang's groups,[47–51] were applied in preparing porphyrin derivatives. Two novel porphyrin derivatives

[a] College of Chemistry and Materials Science, Fujian Normal University, Fuzhou 350007, P. R. China. E-mail: yangfafu@fjnu.edu.cn
[b] Fujian Key Laboratory of Polymer Materials, Fuzhou 350007, P. R. China
[c] Fujian Provincial Key Laboratory of Advanced Materials Oriented Chemical Engineering, Fuzhou 350007, P. R. China

† Electronic supplementary information (ESI) available. See DOI: 10.1039/c9sm01174a

with AIE groups were synthesized and displayed excellent fluorescence in both solution and aggregated states.[52,53] But no porphyrin liquid crystal with fluorescence in both solution and aggregated states was presented up to now. In this paper, the first porphyrin liquid crystal with strong fluorescence in both solution and aggregated states was designed and synthesized by introducing polyglycol-diphenylacrylonitrile units onto the porphyrin skeleton. This novel porphyrin derivative possessed a good self-assembly ability of the liquid–crystalline hexagonal columnar mesophase. Moreover, based on the overlap of the emission wavelength of diphenylacrylonitrile and the absorption wavelength of the porphyrin, a strong FRET (fluorescence resonance energy transfer) effect existed between the diphenylacrylonitrile unit and porphyrin unit. As a result, this novel porphyrin liquid crystal showed strong fluorescence in both solution and aggregated states. The excellent fluorescence property was further successfully applied for fluorescence imaging of living HeLa cells, which was firstly observed for porphyrin liquid crystalline materials.

2. Results and discussion

2.1. Synthesis and characterization

Diphenylacrylonitrile is a classic AIE group with an emission wavelength of 425 nm approximately in the aggregated state,[54] which was overlapped with an absorption wavelength of 420 nm for the porphyrin skeleton. This overlap of wavelengths was favourable for the AIE-FRET effect between diphenylacrylonitrile units and porphyrin skeleton in the aggregated state. On the other hand, the multiple polyglycol chains on the periphery contributed to the production of liquid crystalline properties and enhanced hydrophilicity for increasing the bio-imaging abilities in aqueous solution. The synthetic route is designed as in Scheme 1. The diphenylacrylonitrile derivatives **3**, **4** and **5** were prepared sequentially by using 4-hydroxybenzaldehyde and compound **1** as starting materials. By the classic condensation process of the preparation of the porphyrin skeleton,[55] diphenylacrylonitrile–porphyrin derivative **6** was synthesized in a yield of 8.8% after column chromatography. The structure of target compound **6** was examined by ^{1}H NMR, ^{13}H NMR, MALDI-TOF-MS and elemental analysis. All spectral signals were in agreement with its structure (see the ESI†). For example, the NH of the porphyrin skeleton exhibited a shift at −2.76 ppm in the ^{1}H NMR spectrum, certainly suggesting the formation of the porphyrin skeleton.

2.2. Mesomorphic studies

The mesomorphic self-assembly property of porphyrin **6** was studied by differential scanning calorimetry (DSC), polarizing optical microscopy (POM) and X-ray diffraction (XRD) measurements. Fig. 1 exhibits the DSC curves of porphyrin **6**. The corresponding phase transition temperatures and enthalpy changes are summarized in Table 1. It can be seen that porphyrin **6** possessed two endothermic peaks at 71.4 °C and 118.9 °C upon second heating and two exothermic peaks at 62.2 °C and 115.4 °C during first cooling, respectively. These good reversible phase transition

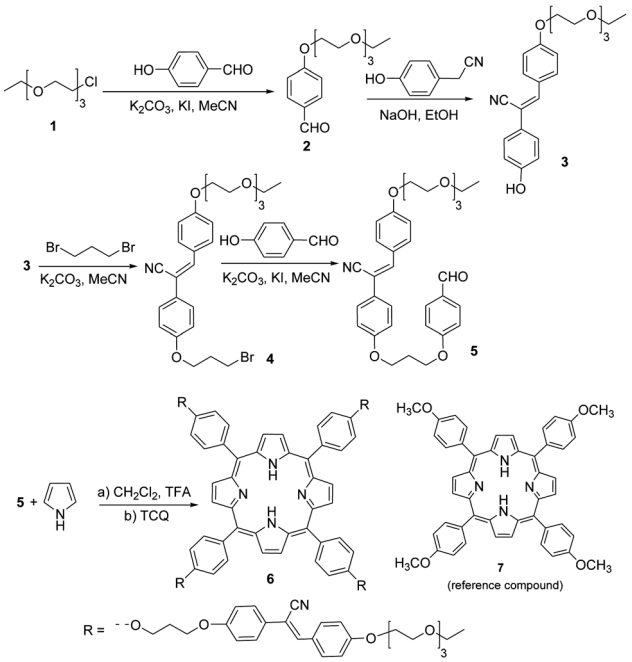

Scheme 1 The synthetic route for title compound **6**.

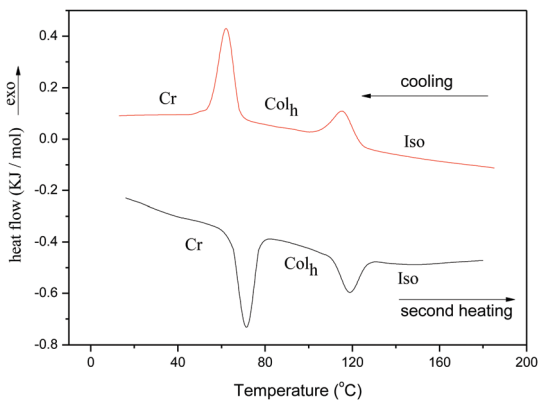

Fig. 1 DSC curves of porphyrin **6** upon second heating and first cooling at a scanning rate of 10 °C min^{-1}.

Table 1 Transition temperatures (°C) and enthalpies (kJ mol^{-1}) of porphyrin **6**

Phase transition[a]	Heating scan $T(\Delta H)$	Cooling scan $T(\Delta H)$
Cr–Col_h(Col_h–Cr)	71.4(17.8)	62.2(16.4)
Col_h–Iso(Iso–Col_h)	118.9(6.5)	115.4(7.3)

[a] Cr = crystalline, Col_h = hexagonal columnar phase, Iso = isotropic.

behaviors corresponded to the crystalline-mesophase-isotropic transition forcefully. The slight hysteresis phenomenon could be rationally attributed to the viscous material with a large molecular weight. Moreover, the mesophase texture of porphyrin **6** was observed under a POM. Obvious phase transitions of Iso–Col and Col–Cr were seen during heating and cooling processes. Fig. 2 displays the mesophase texture at 90 °C upon cooling under POM observation. The typical pseudo-focal conic fan-shape textures

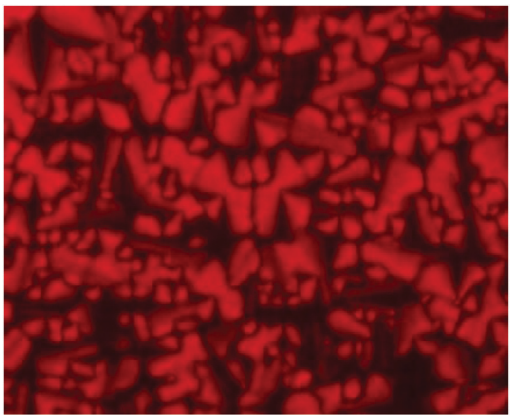

Fig. 2 The mesophase texture of porphyrin **6** at 90 °C upon cooling under POM observation (×400 times).

suggested the ordered hexagonal columnar mesophase for porphyrin **6**, which was further confirmed by following XRD analysis. These results of DSC analysis and POM observation indicated that porphyrin **6** had an excellent self-assembly ability to form a hexagonal columnar phase at 70–120 °C approximately.

Moreover, the molecular stacking behavior of porphyrin **6** was studied by XRD analysis as shown in Fig. 3. It can be seen that a sharp scattering peak at $2\theta = 2.02^\circ$ and three weak peaks ($2\theta = 3.50^\circ$, 4.04° and 5.34°) appeared in the small-angle region, indicating *d*-spacings of 43.73 Å, 25.25 Å, 21.87 Å and 16.53 Å, respectively. The ratio for these *d*-spacings is in accordance with $1:1/\sqrt{3}:1/\sqrt{4}:1/\sqrt{7}$, which can be indexed as the $[d_{100}]$, $[d_{110}]$, $[d_{200}]$ and $[d_{210}]$ planes of a columnar hexagonal mesophase. Also, a broad diffuse halo at $2\theta = 18$–28° with a mean distance of 4.4 Å was observed for the molten alkyl chains in the wide-angle region. These XRD data supported that porphyrin **6** was an ordered self-assembly hexagonal columnar liquid crystal. Moreover, a couple of weak sharp signals (named h_2) between 13.5° and 24.2°, and two weak and broad signals in regions of 9.4°–12.4° (named h_3) and 24.6°–26.4° (named h_1), respectively, could be distinguished. The *d*-spacings for h_1, h_2 and h_3 were 3.3–3.6 Å, 3.6–6.6 Å and 9.3–12.2 Å, approximately. Obviously, h_1 could be attributed to the representative intracolumnar-packing distance of the porphyrin cores. The value of h_3 was nearly triple

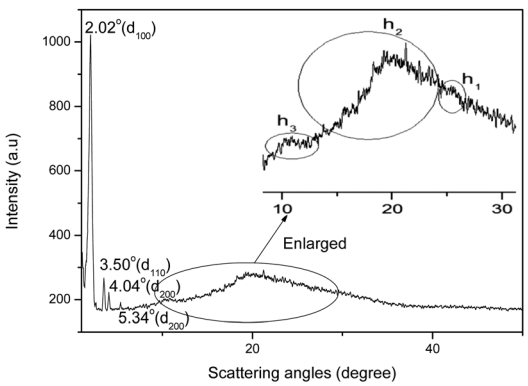

Fig. 3 The XRD trace of porphyrin **6** in the mesophase at 90 °C.

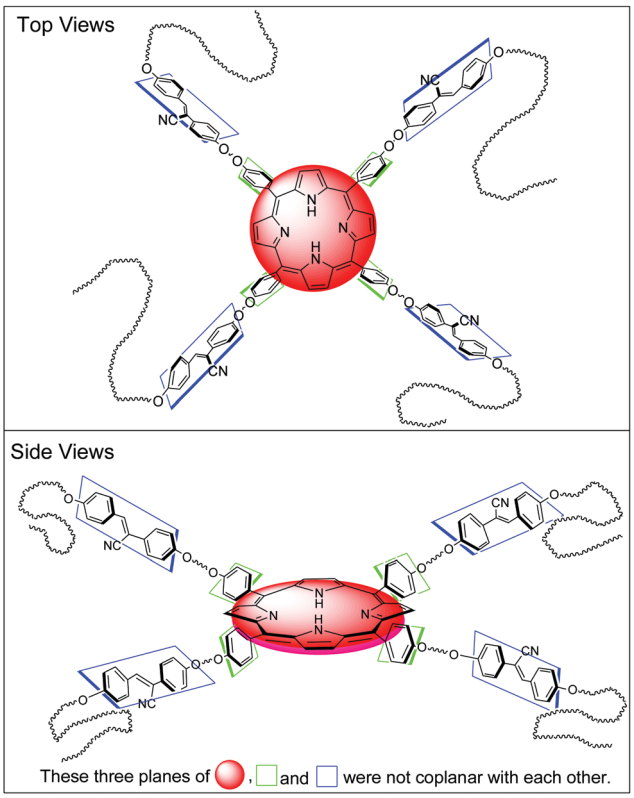

Fig. 4 The preferred conformation of porphyrin **6**.

distance of h_1, indicating some kind of three-molecule associations for the Col_h mesophase of porphyrin **6**. On the other hand, the lattice constant (a) was calculated as 50.50 Å, which was far smaller than the diameter of porphyrin **6** in linear shape (76 Å approximately), suggesting that the alkyl chains might be curled and folded or interdigitated in the mesophase. As previous studies had reported that the beta-octasubstituted porphyrin derivatives prefer the columnar mesophase and the meso-tetrasubstituted porphyrins need to increase the number of alkyl chains to obtain LC mesophases,[56–61] it was reasonable to deduce that the long meso-tetrasubstituted chains of porphyrin **6** adopted the curled and folded shape, which was favourable for producing the LC mesophase. Furthermore, the number (n) of molecules in a single disk of the column could be proposed according to the following formula,[62]

$$n = (a^2)(\sqrt{3}/2)(h\rho N_A/M)$$

where the notation "a" is the hexagonal lattice parameter, N_A is Avogadro's number and M is the molecular mass of the compound. The thickness [h] of the slice is about 3.4 Å estimated by h_1. Due to only four alkyl chains (less than the usual six or eight alkyl chains of the columnar mesophase) on the periphery of porphyrin **6**, the density (ρ) is assumed as 0.7–0.8 g cm^{-3}, which was less than normal ρ values (0.9–1.0 g cm^{-3}).[62] After calculation, the estimated number of molecules (n) in a disk of the columnar hexagonal state was approximately 1 for porphyrin **6**. The estimated number of molecules (n) was nearly 3 when using h_3 for the thickness [h] of the slice. These XRD analyses suggested that the

supramolecular arrangement of the mesophase of porphyrin **6** might be slightly different from the normal hexagonal columnar mesophase.

The literature had confirmed that, for the purpose of an energy-minimized structure, the meso-substituted phenyl groups had a nonplanar conformation with a porphyrin core due to the bulky effect.[63,64] Thus, the possible preferred conformation of porphyrin **6** is proposed in Fig. 4, in which the three planes of the porphyrin core, phenyl groups and diphenylacrylonitrile units were not coplanar with each other, surrounded by curled or folded alkyl chains. Based on Fig. 4, an intracolumnar arrangement of trimolecular stacks per unit cell in the Col_h mesophase is proposed in Fig. 5. Although three porphyrin cores per unit cell were in ordered columnar stacking, the phenyl groups and diphenylacrylonitrile units would stand out of the porphyrin plane and would invade the planar space of neighboring molecules due to the requirements of the minimum-energy conformation and the flexible C_3H_6 spacers. This stable association was comprised of three molecules, with the C_3H_6 spacers mutually holding the neighboring molecules, resulting in the three stacking distances of h_3. The stacking distance of h_1 could be ascribed to rapid thermal fluctuations of the conformations of the disks which eliminates the crystallographic difference among the three disks in a unit cell. The couple of weak sharp signals (h_2) might be attributed to the reflections of low and part order of the layer or columnar arrangement of the phenyl group and diphenylacrylonitrile unit mixed flexible chains. Because the geometry of the trimolecular associations was not well-defined nor their interdistance constant, all the reflections of h_1, h_2 and h_3 were weak and broad signals. Indeed, this kind of trimolecular stack per unit cell for the columnar stacking had been observed in a previous porphyrin liquid crystalline system,[65,66] which also possessed bulky aromatic groups on the peripheral flexible chains of the porphyrin core. On the other hand, it should be clarified that the peripheral alkyl chains of Fig. 5 were in curled, folded or interdigitated disordered arrays with neighboring disks in the hexagonal columnar mesophase.

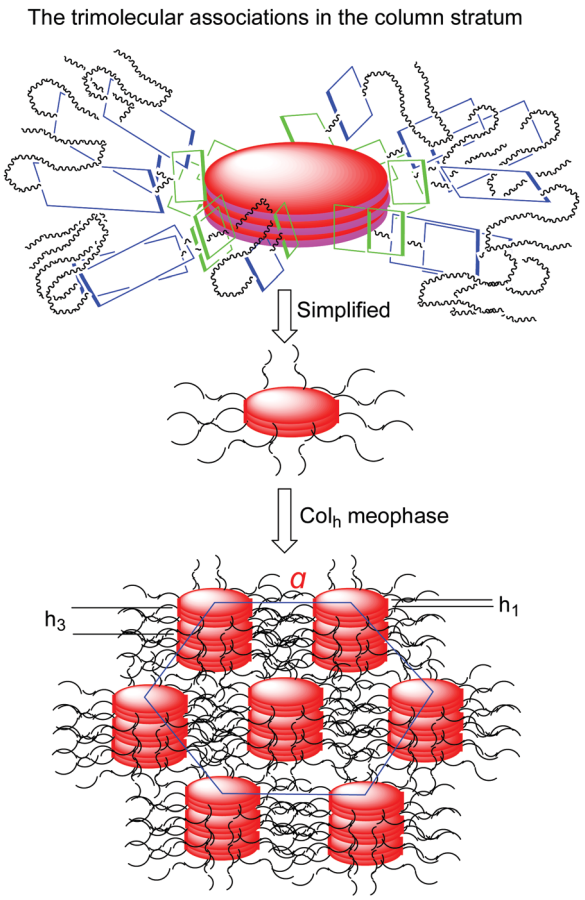

Fig. 5 The proposed molecular stacking mode for the hexagonal columnar mesophase of porphyrin **6**.

2.3. Photophysical studies

The photophysical properties of porphyrin **6** were examined using UV-vis spectra and fluorescence spectra. The porphyrin derivative **7** with an OMe group (without the AIE group, as shown in Scheme 1) was cited as a reference compound for comparison. Fig. 6 illustrates the UV-vis spectra and fluorescence spectra of porphyrins **6** and **7**. One can see that both porphyrins **6** and **7** displayed the absorption peaks at 421, 517, 553, 595 and 652 nm in UV-vis spectra, which were the typical porphyrin absorption Soret bands and four Q bands. Besides, porphyrin **6** showed another strong absorption peak at 320–390 nm (Fig. 6A), which could be ascribed to the absorption of diphenylacrylonitrile units. As to the fluorescence spectra (Fig. 6B), porphyrins **6** and **7** exhibited a similar fluorescence emission (excitation at 420 nm) at 640–760 nm, although the fluorescence intensities fluctuated reasonably. These phenomena were in accordance with the structure of porphyrin **6**, in which the porphyrin unit and diphenylacrylonitrile units were linked by

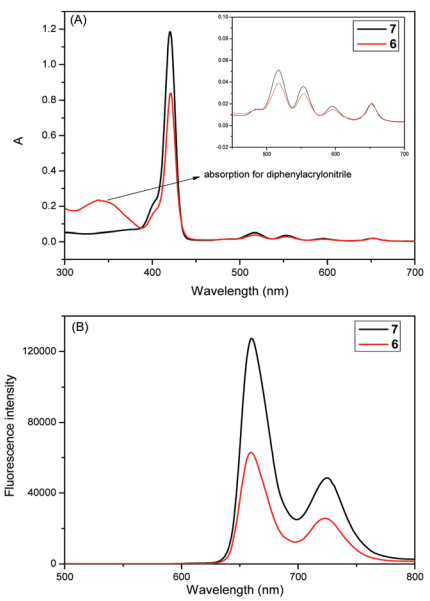

Fig. 6 (A) UV-vis absorption spectra of compounds **6** and **7** (5 μM) and (B) fluorescence spectra (excitation at 420 nm) of compounds **6** and **7** (1 μM) in THF solution.

saturated alkyl chains, resulting in little interaction between these two structural units.

Furthermore, the AIE behaviors of porphyrin **6**, precursor **4** and reference compound **7** were investigated in THF–H_2O mixtures. Precursor **4** exhibited strong fluorescence at 400–500 nm when H_2O fractions were bigger than 80% in THF/H_2O mixtures (see Fig. S11, ESI†), suggesting the good AIE effect for the structure of the diphenylacrylonitrile moiety. As expected, it can be seen that the Soret band absorption of the porphyrin skeleton (400–450 nm) was overlapped with the scope of fluorescence emission (400–500 nm) of diphenylacrylonitrile derivative **4** in the aggregated state, which was favourable for the FRET effect between these two structural units. On the other hand, the reference compound **7** without an AIE group showed no AIE property (see Fig. S12, ESI†). Its fluorescence decreased obviously with the increase of H_2O fraction in THF/H_2O mixtures and almost quenched completely due to the ACQ effect. However, diphenylacrylonitrile–porphyrin derivative **6** exhibited totally different fluorescence properties by comparison with precursor **4** and reference compound **7**. When excited by the Soret band (λ_{ex} = 420 nm), the fluorescence intensities of porphyrin **6** decreased rapidly with the increase of f_w in THF–H_2O solutions, suggesting the strong ACQ effect for the aggregated states (Fig. 7A). The fluorescence of porphyrin **6** was almost quenched completely in the THF–H_2O solution with 90% of H_2O. When excited by the wavelength of the diphenylacrylonitrile unit (λ_{ex} = 350 nm), the fluorescence intensities of porphyrin **6** decreased a little with the increase of f_w from 0% to 40%, and then increased with the increase of f_w from 40% to 90%. The fluorescence in the THF–H_2O solutions with 70–90% of H_2O was even stronger than that in pure THF solution. Moreover, unlike Fig. S11 (ESI†) showing fluorescence changes of precursor **4** in THF–H_2O solutions, no remarkable fluorescence emission was observed for the diphenylacrylonitrile unit in all THF–H_2O solutions of porphyrin **6** (no emission peak at 400–500 nm) (Fig. 7B). Taking into account the outstanding AIE effect of precursor **4** in THF/H_2O solution (λ_{ex} = 350 nm), the strong fluorescence of porphyrin **6** in THF/H_2O solution (λ_{ex} = 350 nm) could be attributed to the AIE effect of diphenylacrylonitrile units and the FRET process between diphenylacrylonitrile and porphyrin units. As a result, no fluorescence at 400–500 nm appeared for diphenylacrylonitrile units and excellent fluorescence was produced in all THF–H_2O solutions for porphyrin **6**. Based on these results, a subtle balance could be deduced for the ACQ effect and AIE-FRET effect. When $f_w < 40\%$, the ACQ effect suppressed the AIE and FRET effect, causing a decrease of fluorescence. When $f_w > 40\%$, the AIE-FRET effect increased rapidly and became stronger than the ACQ effect, resulting in a strong fluorescence in the aggregated state.

In order to confirm further the AIE-FRET effect in the aggregated state, the fluorescence spectra of porphyrin **6** in the solid state and mesophase film and reference compound **7** in the solid state were studied as exhibited in Fig. 8. It could be seen that porphyrin **6** displayed similar fluorescence spectra in the solid state and mesophase film with the strong fluorescence emission at the near-infrared region (650–750 nm). A little red shift for porphyrin **6** in the mesophase film might suggest the

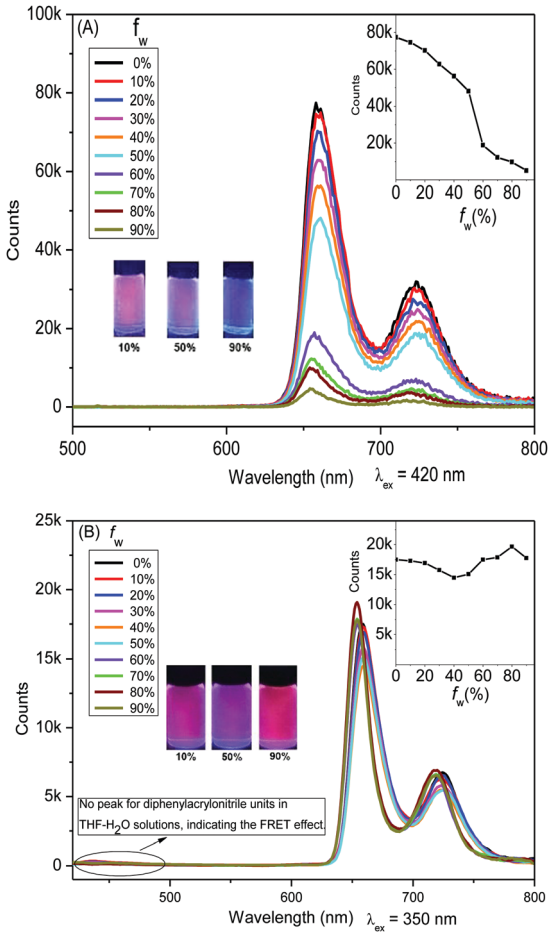

Fig. 7 (A) The fluorescence spectra of porphyrin **6** (1 μM) in the THF/water mixture with different water fractions (excitation at 420 nm). (B) The fluorescence spectra of porphyrin **6** (1 μM) in the THF/water mixture with different water fractions (excitation at 350 nm). Inset: The line plot of fluorescence intensity change from 0–90% water fractions of porphyrin **6** and the fluorescence photos (under UV_{365} light) of porphyrin **6** in THF/water mixtures at f_w = 10%, 50% and 90%, respectively.

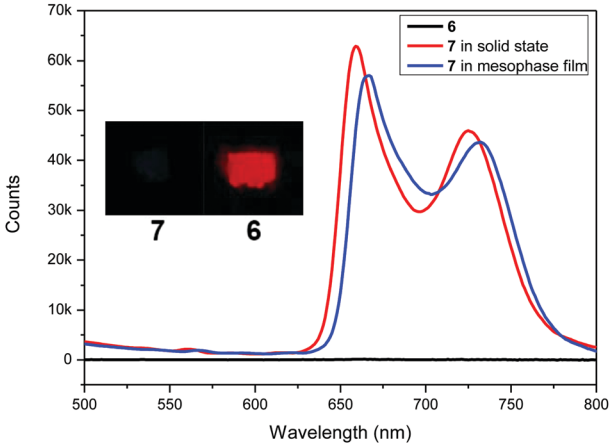

Fig. 8 The fluorescence spectra of porphyrins **6** (solid state), **7** (solid state) and **7** (mesophase film) (excitation at 350 nm). Inset: The fluorescence photos of porphyrins **6** and **7** in the solid state.

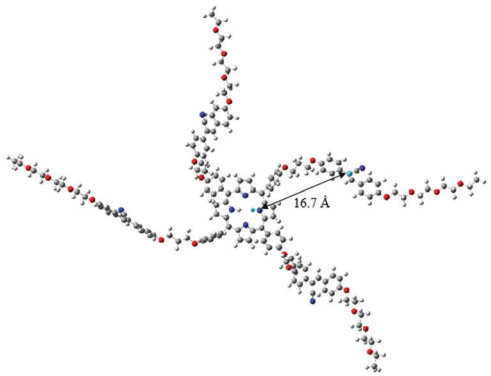

Fig. 9 The optimized structure of porphyrin **6** based on the DFT calculation.

J-aggregation in the mesophase state. But reference compound **7** showed no obvious emission. The inserted fluorescence pictures also suggested no fluorescence for compound **7** but a strong red fluorescence for porphyrin **6**. This comparison in solid emission certainly also supported the existence of the AIE-FRET effect between diphenylacrylonitrile and porphyrin moieties of porphyrin **6**. The pseudo Stokes shift of porphyrin **6** was as large as 210 nm. The fluorescence quantum yield was 0.12 in the solid state, which was outstanding among porphyrin derivatives. On the other hand, the distance between diphenylacrylonitrile and porphyrin moieties of porphyrin **6** was calculated as 16.7 Å based on the DFT calculation (as shown in Fig. 9), which was suitable for producing the FRET effect. Thus, the emission mechanism in the aggregated state for porphyrin **6** is proposed in Fig. 10.

2.4. Fluorescence imaging of porphyrin 6

Although normal porphyrins showed good near-infrared emission, they were limited to apply for bio-imaging in aqueous solution due to the strong ACQ effect. As diphenylacrylonitrile–porphyrin derivative **6** displayed excellent fluorescence in solution and the aggregated state based on the AIE-FRET effect, it was expected to exhibit the bio-imaging ability in aqueous solution. Thus, fluorescence imaging of porphyrin **6** *in vitro* HeLa cells was examined using a fluorescence inverted microscope. After incubation with porphyrin **6** for 2 h at 37 °C, the HeLa cells were rinsed with PBS solution. Later, the cells were fastened and observed under an inverted microscope (Leica inverted microscope

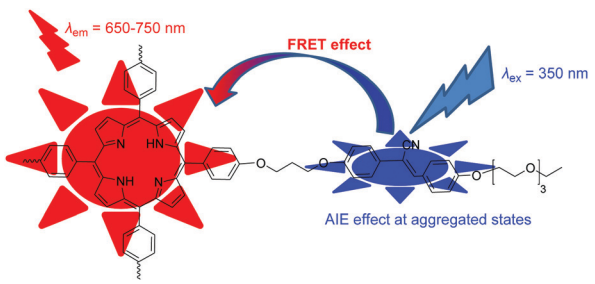

Fig. 10 The proposed illustration of the AIE-FRET effect for porphyrin **6**.

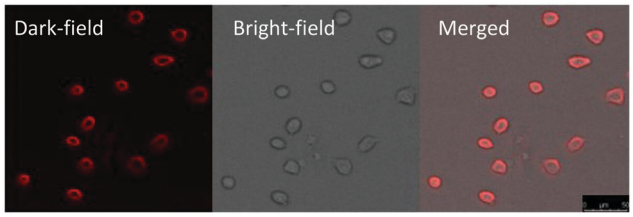

Fig. 11 Dark-field image (left), bright-field image (middle) and the merged images of dark and bright fields (right). λ_{ex} = 460–550 nm. Scale bar: 50 μm.

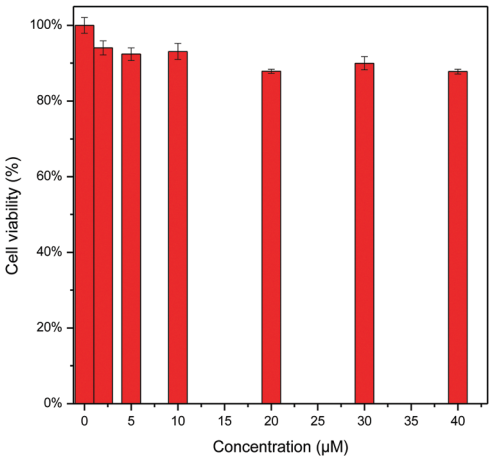

Fig. 12 Relative cell viabilities of HeLa cells incubated with different concentrations of porphyrin **6** for 24 h.

DM IL LED). The G-type excitation/emission components of this instrument (excitation chip wavelength: 460–550 nm, emission chip wavelength: 590 nm) were applied to study the red fluorescence cell imaging for porphyrin **6**. As expected, the strong red fluorescence imaging was observed for HeLa cells with porphyrin **6** (Fig. 11), indicating the excellent bio-imaging performance of porphyrin **6** in aqueous solution. On the other hand, the HeLa cell metabolic activity of porphyrin **6** with MTT assay was investigated as shown in Fig. 12. The cell viabilities were over 90% at 0–40 μM in 24 h, suggesting the low biotoxicity for porphyrin **6**. The excellent bio-imaging ability of porphyrin **6** might be attributed to not only the good near-infrared emission in aggregated states but also the good biocompatibility of multiple polyglycol chains on the periphery. In a word, these results indicated that the novel diphenylacrylonitrile–porphyrin derivative **6** possessed an excellent application potential for near-infrared fluorescence bioimaging in living cells.

3. Conclusions

In conclusion, a novel diphenylacrylonitrile–porphyrin derivative with multiple polyglycol chains on the periphery was designed and prepared as the near-infrared-emissive fluorescence liquid crystalline material in both solution and aggregated states. The DSC, POM and XRD studies showed that it had excellent self-assembly ability with the ordered hexagonal

columnar mesophase between 70 and 120 °C approximately. The investigation of the photophysical properties indicated that the novel porphyrin liquid crystal had excellent emission in both solution and aggregated states. When excited by the wavelength of the diphenylacrylonitrile unit, the fluorescence intensities maintained a high level, which were attributed to the cooperative mechanism of AIE and FRET effects between the diphenylacrylonitrile unit and porphyrin unit based on the overlap of the emission of diphenylacrylonitrile and the absorption of the porphyrin. The pseudo Stokes shift of the novel porphyrin liquid crystal was as large as 210 nm and the fluorescence quantum yield was 0.12 in the solid state. Moreover, it exhibited low biotoxicity and excellent fluorescence bio-imaging ability in living cells. In a word, this paper reported the first porphyrin liquid crystal with excellent near-infrared emission in both solution and aggregated states as well as good fluorescence imaging ability and biocompatibility in living cells, which provided a good strategy for the design and synthesis of novel near-infrared material with excellent self-assembly properties and high fluorescence in both solution and solid states for application in the bioimaging of living cells.

4. Experimental section

4.1. General

All chemical reagents were supplied by Aladdin Reagent Co., Ltd. and used without further purification. The other organic solvents and inorganic reagents were purified by standard anhydrous methods before use. TLC analysis was carried out by using pre-coated glass plates. Column chromatography was done by using silica gel (200–300 mesh). NMR spectra were measured on a Bruker-ARX 400 instrument at 26 °C. Chemical shifts are reported in ppm with tetramethylsilane (TMS) as an internal standard. MS spectra were recorded on a Bruker mass spectrometer. DSC measurements were examined on a Thermal Analyzer Q100 at a scanning rate of 10 °C min^{-1} under an N_2 atmosphere. Mesomorphic texture was observed using a polarization optical microscope (Leica DMRX) equipped with a temperature-controlled heating stage (Linkam THMSE 600). X-ray diffraction (XRD) experiments were performed on a SEIFERT-FPM (XRD7) diffraction meter using Cu Kα radiation (λ = 1.5406 Å) with 40 kV, 30 mA power. UV-Vis spectra were measured on a Varian UV-Vis spectrometer. Fluorescence spectra were recorded in a conventional quartz cell (10 × 10 × 45 mm) at 25 °C on an Edinburgh Instruments FS5 spectrometer. The fluorescence absolute Φ_F values were studied on an Edinburgh Instruments FLS920 Fluorescence Spectrometer with a 6 inch integrating sphere.

4.2. Synthesis of compound 2

A mixture of 4-hydroxybenzaldehyde (0.4 g, 2.0 mmol), compound **1** (0.25 g, 2.0 mmol), K_2CO_3 (0.5 g, 3.7 mmol) and KI (0.1 g, 0.6 mmol) in 40 mL of dry MeCN was stirred and refluxed for 12 h. After reaction and cooling, 20 mL of HCl solution (1 M) and 40 mL of $CHCl_3$ were added. Then the $CHCl_3$ layer was partitioned, washed with 20 mL of distilled water, dried over anhydrous $MgSO_4$, and concentrated. The residue was further purified by rapid column chromatography using CH_2Cl_2/hexane (1 : 1, v/v) as an eluent. Compound **2** was collected as a sticky solid in a yield of 82%. ^{1}H NMR (400 MHz, $CDCl_3$) δ: 9.88 (s, 1H, CHO), 7.83 (d, J = 8.0 Hz, 2H, ArH), 7.03 (d, J = 8.0 Hz, 2H, ArH), 4.22 (t, J = 4.0 Hz, 2H, OCH_2), 3.90 (t, J = 4.0 Hz, 2H, OCH_2), 3.64–3.78 (m, 10H, OCH_2), 1.23 (t, J = 4.0 Hz, 3H, CH_3).

4.3. Synthesis of compound 3

A mixture of 4-hydroxyphenylacetonitrile (0.14 g, 1.0 mmol), compound **2** (0.28 g, 1.0 mmol) and NaOH (0.10 g, 2.5 mmol) in 30 mL of EtOH solution was stirred for 10 h at room temperature. The reaction was monitored by the TLC technique, suggesting the disappearance of the materials. After reaction, 10 mL of HCl solution (1 M) was poured into the reaction mixture. The precipitate was formed and filtered. The obtained precipitate was purified by recrystallization in MeOH/CH_2Cl_2 (1 : 1, v/v). After dryness, compound **3** was obtained as a pale yellow solid in a yield of 78%. ^{1}H NMR (400 MHz, DMSO) δ: 9.91 (s, 1H, OH), 7.91 (d, J = 12.0 Hz, 2H, ArH), 7.78 (s, 1H, C═CH), 7.57 (d, J = 8.0 Hz, 2H, ArH), 7.26 (d, J = 8.0 Hz, 2H, ArH), 6.88 (d, J = 8.0 Hz, 2H, ArH), 4.18 (t, J = 4.0 Hz, 2H, OCH_2), 3.78 (t, J = 4.0 Hz, 2H, OCH_2), 3.40–3.61 (m, 10H, OCH_2), 1.10 (t, J = 8.0 Hz, 3H, CH_3); MALDI-TOF-MS ($C_{23}H_{27}NO_5$) calcd for m/z = 397.19, found: m/z = 399.04 (MH^+), 421.20 (MNa^+), 437.63 (MK^+).

4.4. Synthesis of compound 4

Under an N_2 atmosphere, a mixture of compound **3** (0.40 g, 1.0 mmol), 1,3-dibromopropane (0.4 g, 2 mmol), and K_2CO_3 (0.36 g, 2.6 mmol) was stirred and refluxed in 30 mL of dry MeCN for 20 h. The reaction was monitored by the TLC technique implying the disappearance of reactants. After reaction, the mixture was treated with 50 mL of HCl (1 M) and extracted with 30 mL of $CHCl_3$. The $CHCl_3$ layer was partitioned, washed with 20 mL of distilled water, dried over anhydrous $MgSO_4$, and then concentrated. The residue was treated with 15 mL of MeOH and the precipitate was obtained. The crude product was further purified by recrystallization in MeOH/CH_2Cl_2 (2 : 1, v/v). After dryness, compound **4** was collected as a pale yellow solid in a yield of 69%. ^{1}H NMR (400 MHz, $CDCl_3$) δ: 7.83 (d, J = 8.0 Hz, 2H, ArH), 7.57 (d, J = 8.0 Hz, 2H, ArH), 7.34 (s, 1H, C═CH), 6.97 (d, J = 8.0 Hz, 2H, ArH), 6.94 (d, J = 8.0 Hz, 2H, ArH), 3.50–4.19 (m, 18H, OCH_2), 2.30–2.36 (m, 2H, CH_2), 1.20 (t, J = 8.0 Hz, 3H, CH_3); MALDI-TOF-MS ($C_{26}H_{32}NO_5$) calcd for m/z = 519.14, found: m/z = 520.01 (MH^+).

4.5. Synthesis of compound 5

Under an N_2 atmosphere, a mixture of compound **4** (0.52 g, 1.0 mmol), 4-hydroxybenzaldehyde (0.20 g, 1.6 mmol) and K_2CO_3 (0.28 g, 2.0 mmol) was stirred and refluxed in 25 mL of dry MeCN for 24 h. The reaction was monitored by the TLC technique implying the disappearance of reactants. After reaction, the mixture was treated with 30 mL HCl (1 M) and extracted with 30 mL of $CHCl_3$. The $CHCl_3$ layer was partitioned, washed with 15 mL of distilled water, dried over anhydrous $MgSO_4$, and then concentrated. The residue was treated with 15 mL of MeOH and the precipitate was obtained. The crude product was further

purified by column chromatography using CH_2Cl_2/hexane (1 : 1, v/v) as an eluent. After dryness, compound **5** was obtained as a pale yellow solid in a yield of 82%. ^{1}H NMR (400 MHz, $CDCl_3$) δ: 9.87 (s, 1H, CHO), 7.83 (d, J = 8.0 Hz, 4H, ArH), 7.56 (d, J = 8.0 Hz, 2H, ArH), 7.33 (s, 1H, C═CH), 6.93–7.03 (m, 6H, ArH), 3.48–4.27 (m, 18H, OCH_2), 2.28–2.34 (m, 2H, CH_2), 1.20 (t, J = 8.0 Hz, 3H, CH_3). MALDI-TOF-MS ($C_{33}H_{37}NO_7$) calcd for m/z = 559.65, found: m/z = 561.47 (MH^+).

4.6. Synthesis of compound 6

A mixture of compound **5** (0.56 g, 1 mmol) and pyrrole (67 mg, 1 mmol) was stirred for 60 min at room temperature in 100 mL of CH_2Cl_2 with 0.3 mL of trifluoroacetic acid (TFA), followed by oxidation with tetrachlorobenzoquinone (TCQ) (197 mg, 0.8 mmol). After reaction, the solvent was removed using a rotary evaporator. The crude product was further purified by silica chromatography on silica gel (eluent: $CHCl_2$/ethyl acetate = 85/15), affording compound **6** in 8.8% yield as a purple solid. ^{1}H NMR (400 MHz, $CDCl_3$) δ ppm: 8.85 (s, 8H, pyrrole CH), 8.11 (d, J = 8.0 Hz, 8H, ArH), 7.33 (d, J = 8.0 Hz, 8H ArH), 7.63 (d, J = 8.0 Hz, 8H, ArH), 7.36 (s, 4H, C═CH), 7.29 (d, J = 8.0 Hz, 8H, ArH), 7.06 (d, J = 8.0 Hz, 8H, ArH), 6.96 (d, J = 8.0 Hz, 8H, ArH), 3.50–4.47 (m, 72H, OCH_2), 2.49 (t, J = 4.8 Hz, 8H, CH_2), 1.21 (t, J = 8.0 Hz, 12H, CH_3), −2.76 (s, 2H, pyrrole NH); ^{13}C NMR (100 MHz, $CDCl_3$) δ ppm: 15.18, 29.56, 64.63, 64.81, 66.66, 67.58, 69.60, 69.84, 70.67, 70.76, 70.91, 108.39, 112.68, 114.60, 114.85, 118.69, 119.74, 126.76, 127.18, 127.55, 130.30, 130.87, 131.40, 134.79, 135.64, 139.98, 158.15, 158.62, 160.35; MALDI-TOF-MS ($C_{148}H_{154}N_8O_{24}$) calcd for m/z = 2428.11, found: m/z = 2429.67 (MH^+). Anal. calcd for $C_{148}H_{154}N_8O_{24}$: C, 73.19; H, 6.39; N, 4.61. Found: C, 73.15; H, 6.44; N, 4.52.

4.7. Cell cultivation and fluorescence imaging

Compound **6** was dissolved in THF solution (0.5 mg mL^{-1}). By vigorous stirring at room temperature, this solution (0.4 mL) was quickly dropwise dispersed into 25 mM solution of $NaHCO_3$ (4 mL). Then the solution was stirred overnight at room temperature to remove THF and stored for further fluorescence imaging. HeLa cells were cultured in a 6-well plate with a density of 2×10^5 cells per well and incubated in DMEM for 24 h. Later, porphyrin **6** was incubated with HeLa cells for 2 h at 37 °C. HeLa cells were washed with PBS three times. Finally, the cells were fixed by methanol for 10 min at −20 °C and observed under an inverted microscope (Leica inverted microscope DM IL LED).

Conflicts of interest

There are no conflicts to declare.

Acknowledgements

Financial support from the National Natural Science Foundation of China (No. 21406036), the Fujian Natural Science Foundation of China (No. 2017J01571), the Fujian Science and Technology Project (No. 2019N0010), the Fuzhou Science and Technology Project (2018-G-44), and the Undergraduate innovation program of FJNU (2019) was greatly acknowledged.

References

1 T. Wöhrle, I. Wurzbach, J. Kirres, A. Kostidou, N. Kapernaum, J. Litterscheidt, J. C. Haenle, P. Staffeld, A. Baro, F. Giesselmann and S. Laschat, *Chem. Rev.*, 2016, **116**, 1139–1241.
2 S. Kumar, *Chemistry of discotic liquid crystals: from monomers to polymers*, CRC, Taylor and Francis Group, LLC, 2011.
3 T. Nakanishi, *Functional organic liquids*, Wiley-VCH Verlag GmbH & Co. KGaA, 2019.
4 S. Laschat, A. Baro, N. Steinke, F. Giesselmann, C. Hagele, G. Scalia, R. Judele, E. Kapatsina, S. Sauer, A. Schreivogel and M. Tosoni, *Angew. Chem., Int. Ed.*, 2007, **46**, 4832–4887.
5 S. Sergeyev, W. Pisula and Y. H. Geerts, *Chem. Soc. Rev.*, 2007, **36**, 1902–1929.
6 S. K. Pal, S. Setia, B. S. Avinash and S. Kumar, *Liq. Cryst.*, 2013, **40**, 1769–1816.
7 F. F. Yang, H. Y. Guo and J. Vicens, *J. Inclusion Phenom. Macrocyclic Chem.*, 2014, **80**, 177–186.
8 E. K. Fleischmann and R. Zentel, *Angew. Chem., Int. Ed.*, 2013, **52**, 8810–8827.
9 T. Yasuda, H. Ooi, J. Morita, Y. Akama, K. Minoura, M. Funahashi, T. Shimomura and T. Kato, *Adv. Funct. Mater.*, 2009, **19**, 411–419.
10 X. Q. Li, X. Zhang, S. Ghosh and F. Würthner, *Chem. – Eur. J.*, 2008, **14**, 8074–8078.
11 X. T. Fang, H. Y. Guo, J. R. Lin and F. F. Yang, *Tetrahedron Lett.*, 2016, **57**, 4939–4943.
12 A. Florian, M. J. Mayoral, V. Stepanenko and G. Fernandez, *Chem. – Eur. J.*, 2012, **18**, 14957–14961.
13 H. Y. Feng, X. T. Geng, J. R. Lin, H. Y. Guo and F. F. Yang, *Liq. Cryst.*, 2018, **45**, 1470–1476.
14 X. T. Fang, H. Y. Guo, F. F. Yang and J. R. Lin, *RSC Adv.*, 2017, **7**, 23657–23662.
15 A. Wicklein, A. Lang, M. Muth and M. Thelakkat, *J. Am. Chem. Soc.*, 2009, **131**, 14442–14453.
16 L. Meng, Q. M. Wu, F. F. Yang and H. Y. Guo, *New J. Chem.*, 2015, **39**, 72–76.
17 R. K. Gupta, D. S. S. Rao, S. K. Prasad and A. S. Achalkumar, *Chem. – Eur. J.*, 2018, **24**, 3566–3575.
18 H. Y. Guo, M. G. Zhu, Z. S. Wang and F. F. Yang, *Tetrahedron Lett.*, 2016, **57**, 4191–4195.
19 S. Herbst, B. Soberats, P. Leowanawat, M. Lehmann and F. Würthner, *Angew. Chem., Int. Ed.*, 2017, **129**, 2194–2197.
20 M. G. Zhu, Y. Z. Zhuo, H. Y. Guo, F. F. Yang and J. B. Qiu, *J. Lumin.*, 2018, **194**, 264–270.
21 F. Nolde, W. Pisula, S. Müller, C. Kohl and K. Müllen, *Chem. Mater.*, 2006, **18**, 3715–3725.
22 M. G. Zhu, Y. Z. Zhuo, H. Y. Guo, F. F. Yang and X. C. Song, *New J. Chem.*, 2018, **42**, 8998–9007.
23 D. M. P. de, O. Santos, M. G. B. Cabral, A. Bentaleb, R. Cristiano, H. Gallardo, F. Durola and H. Bock, *Chem. – Eur. J.*, 2016, **22**, 7389–7393.

24 M. G. Zhu, Y. X. Chen, X. Y. Zhang, M. H. Chen, H. Y. Guo and F. F. Yang, *Soft Matter*, 2018, **14**, 6737–6744.
25 R. Cristiano, H. Gallardo, A. J. Bortoluzzi, I. H. Bechtold, C. E. M. Campos and R. L. Longo, *Chem. Commun.*, 2008, 5134–5136.
26 S. Glang, T. Rieth, D. Borchmann, I. Fortunati, R. Signorini and H. Detert, *Eur. J. Org. Chem.*, 2014, 3116–3126.
27 A. Santoro, A. M. Prokhorov, V. N. Kozhevnikov, A. C. Whitwood, B. Donnio, J. A. G. Williams and D. W. Bruce, *J. Am. Chem. Soc.*, 2011, **133**, 5248–5251.
28 C. T. Liao, H. H. Chen, H. F. Hsu, A. Poloek, H. H. Yeh, Y. Chi, K. W. Wang, C. H. Lai, G. H. Lee and C. W. Shih, *Chem. – Eur. J.*, 2011, **17**, 546–556.
29 Y. Ni and J. S. Wu, *Org. Biomol. Chem.*, 2014, **12**, 3774–3793.
30 G. Qian and Z. Y. Wang, *Chem. – Asian J.*, 2010, **5**, 1006–1010.
31 A. R. Battersby and E. McDonald, *Acc. Chem. Res.*, 1979, **12**, 14–22.
32 G. C. Shearman, G. Yahioglu, J. Kirstein, L. R. Milgrom and J. M. Seddon, *J. Mater. Chem.*, 2009, **19**, 598–604.
33 S. Sengupta, S. Uemura, S. Patwardhan, V. Huber, F. C. Grozema, L. D. A. Siebbeles, U. Baumeister and F. Würthner, *Chem. – Eur. J.*, 2011, **17**, 5300–5310.
34 M. Stępien, B. Donnio and J. L. Sessler, *Chem. – Eur. J.*, 2007, **13**, 6853–6863.
35 D. Mysliwiec, B. Donnio, P. J. Chmielewski, B. Heinrich and M. Stępień, *J. Am. Chem. Soc.*, 2012, **134**, 4822–4833.
36 B. Wu, K. Chen, Y. Deng, J. Chen, C. Liu, R. Cheng and D. Chen, *Chem. – Eur. J.*, 2015, **21**, 3671–3681.
37 S. W. Kang, Q. Li, B. D. Chapman, R. Pindak, J. O. Cross, L. Li, M. Nakata and S. Kumar, *Chem. Mater.*, 2007, **19**, 5657–5663.
38 T. Sakurai, K. Shi, H. Sato, K. Tashiro, A. Osuka, A. Saeki, S. Seki, S. Tagawa, S. Sasaki and H. Masunaga, *J. Am. Chem. Soc.*, 2008, **130**, 13812–13813.
39 S. Tanaka, T. Sakurai, Y. Honsho, A. Saeki, S. Seki, K. Kato, M. Takata, A. Osuka and T. Aida, *Chem. – Eur. J.*, 2012, **18**, 10554–10561.
40 H. Kayal, M. M. Ahmida, S. Dufour, H. Taing and S. H. Eichhorn, *J. Mater. Chem. C*, 2013, **1**, 7064–7072.
41 M. Stępień, B. Donnio and J. L. Sessler, *Angew. Chem., Int. Ed.*, 2007, **46**, 1431–1435.
42 A. Nowak-Król, D. Gryko and D. T. Gryko, *Chem. – Asian J.*, 2010, **5**, 714–716.
43 S. Maruyama, K. Sato and H. Iwahashi, *Chem. Lett.*, 2010, **39**, 714–716.
44 A. D. Bromby, W. H. Kan and T. C. Sutherland, *J. Mater. Chem.*, 2012, **22**, 20611–20617.
45 J. W. Goodby, P. S. Robinson, B. K. Teo and P. E. Cladi, *Mol. Cryst. Liq. Cryst.*, 1980, **56**, 303–309.
46 D. W. Bruce, M. A. Wali and Q. M. Wang, *Chem. Commun.*, 1994, 2089–2090.
47 Y. Hong, J. W. Y. Lam and B. Z. Tang, *Chem. Soc. Rev.*, 2011, **40**, 5361–5388.
48 H. Wang, E. Zhao, J. W. Y. Lam and B. Z. Tang, *Mater. Today*, 2015, **18**, 365–377.
49 D. Ding, K. Li, B. Liu and B. Z. Tang, *Acc. Chem. Res.*, 2013, **11**, 2441–2453.
50 R. T. Kwok, C. W. Leung, J. W. Y. Lam and B. Z. Tang, *Chem. Soc. Rev.*, 2015, **13**, 4228–4238.
51 Y. Yuan, C. J. Zhang, M. Gao, R. Y. Zhang, B. Z. Tang and B. Liu, *Angew. Chem., Int. Ed.*, 2015, **6**, 1780–1786.
52 B. Guo, X. Cai, S. Xu, S. M. A. Fateminia, J. Liu, J. Liang, G. Feng, W. Wu and B. Liu, *J. Mater. Chem. B*, 2016, **4**, 4690–4695.
53 C. Y. Han, S. J. Jiang, J. B. Qiu, H. Y. Guo and F. F. Yang, *New J. Chem.*, 2019, **43**, 3317–3322.
54 L. Lin, X. Lin, H. Guo and F. Yang, *Org. Biomol. Chem.*, 2017, **15**, 6006–6013.
55 J. S. Lindsey, I. C. Schreiman, H. C. Hsu, P. C. Kearney and A. M. Marguerettaz, *J. Org. Chem.*, 1987, **52**, 827–836.
56 A. Segade, M. Castella, F. López-Calahorra and D. Velaco, *Chem. Mater.*, 2005, **17**, 5366–5374.
57 B. A. Gregg, M. A. Fox and A. J. Bard, *Chem. Commun.*, 1987, 1134–1135.
58 B. A. Gregg, M. A. Fox and A. J. Bard, *J. Am. Chem. Soc.*, 1989, **111**, 3024–3029.
59 M. A. Fox, J. V. Grant, D. Melamed, T. Torimoto, C. Y. Liu and A. J. Bard, *Chem. Mater.*, 1998, **10**, 1771–1776.
60 V. Paganuzzi, P. Guatteri, P. Riccardi, T. Sacchelli, J. Barberá, M. Costa and E. Dalcanale, *Eur. J. Org. Chem.*, 1999, 1527–1539.
61 L. R. Milgrom, G. Yahioglu, D. W. Bruce, S. Morrone, F. Z. Henari and W. J. Blau, *Adv. Mater.*, 1997, **9**, 313–316.
62 K. Ohta, N. Yamaguchi and I. Yamamoto, *J. Mater. Chem.*, 1998, **8**, 2637–2650.
63 J. Li, H. Xin and M. Li, *Liq. Cryst.*, 2006, **33**, 913–919.
64 T. Nakai, K. Ban, K. Ohta and M. Kimura, *J. Mater. Chem.*, 2002, **12**, 844–850.
65 A. Segade, M. Castella, F. López-Calahorra and D. Velasco, *Chem. Mater.*, 2005, **17**, 5366–5374.
66 H. Miwa, N. Kobayashi, K. Ban and K. Ohta, *Bull. Chem. Soc. Jpn.*, 1999, **72**, 2719–2728.